Influence Mechanism and Imaging Effect of Liujunzi Decoction Combined with Network Pharmacology in Intervention of Breast Cancer

YANSHU JIA[1], YINGJI LI[2,*], VIJAY KOTRA[1,*]
[1]Faculty of Pharmacy,
Quest International University,
Ipoh 30250,
MALAYSIA

[2]School of Humanities and Management,
Yunnan University of Chinese Medicine,
Kunming 650500,
CHINA

**Corresponding Author*

Abstract: - **Objective** To reveal the potential molecular mechanism of Liujunzi Decoction (LD) for Breast Cancer (BC) intervention built on network pharmacology, verify its clinical efficacy through imaging evaluation, and explore the response difference of different molecular types of BC to LD. **Methods:** The active ingredients and targets of LD were screened through the TCMSP; Integrating GeneCards, OMIM, and other databases, BC related targets were gained; The network of "Liujunzi Decoction - Components - Target Protein - Breast Cancer" was constructed, and the enrichment analysis of gene ontology/Kyoto gene and genome encyclopedia was carried out. AutoDock was used to verify the binding activity between core components and key targets; An interactive analysis platform based on gene expression levels and Kaplan-Meier Plotter was used to analyze prognostic gene expression. 500 BC cases were included. The consistency, sensitivity, and specificity of the therapeutic effect of LD after intervention were evaluated by dynamic enhanced MRI scanning. **Results:** LD and BC had several common targets, including proto-oncogene activator protein, cell tumor antigen p53, mitogen-activated protein kinase 3, etc. The results of gene ontology analysis demonstrated that biological process items mainly include RNA-pII-PTR, PRoCP, and angiogenesis; The cellular components mainly included dendrites, nuclei, cytoplasm, etc. The molecular functions mainly included protein binding, transcription factor binding, ubiquitin protein ligase binding, etc. The Kyoto Encyclopedia of Genes and Genomes pathway enrichment analysis showed that the cancer pathway had the highest degree of gene enrichment, at 58. In the imaging evaluation results, after intervention with LD, the consistency of MRI detection was high at 83.0%, but the specificity was low at 28.4%. The intervention response of BC patients with different molecular types to LD was significantly different. HR+/HER2 subtype MRI had the highest diagnostic consistency, the highest positive predictive value, and the lowest negative predictive value. **Conclusion:** This study confirms that LD can intervene in BC through multi-component, multi-target, and multi-channel synergistic action, and imaging technology can directly reflect its therapeutic effect.

Key-Words: - Network pharmacology; Imaging; Liujunzi Decoction; BC; Magnetic resonance imaging.

Received: April 14, 2026. Revised: May 16, 2026. Accepted: June 18, 2026. Published: November 20, 2026.

1 Introduction

Breast Cancer (BC) is the most common kind of cancer among women in the world, and also the 2nd most common cancer in the world [1]. In 2025, the International Agency for Research on Cancer, a subsidiary of the WHO, released a report in the journal Nature Medicine on April 24, stating that global cases of BC are expected to rise by 38% by 2050, and the number of deaths from the disease is expected to increase by 68% annually [2]. The complex molecular mechanisms and heterogeneity of BC pose challenges to clinical treatment, such as drug resistance and recurrence. Traditional Chinese Medicine (TCM), with its unique advantages of

multi-target and multi-pathway synergistic regulation, has shown great potential in the comprehensive treatment of tumors. Liujunzi Decoction (LD) has the effects of invigorating the spleen and qi, resolving phlegm, and dispersing nodules [3], [4]. Previous clinical observations have shown that it can enhance postoperative immune function and quality of life in BC patients, but the specific intervention mechanism is still unclear. As an emerging discipline, Network Pharmacology (NetP) can integrate the chemical components, targets, and disease pathways of TCM through systems biology and bioinformatics technologies, revealing the potential mechanisms of TCM formulas from a holistic perspective [5].

The heading of each section should be printed in small, 14pt, left justified, bold, Times New Roman. You must use numbers 1, 2, 3, … for the sections' numbering and not Latin numbering (I, II, III, …)

For example, analyzed the treatment outcomes and prognostic factors of non-metastatic metaplastic BC patients through a multicenter retrospective cohort study, providing a new perspective for the clinical treatment of BC [6]. Imaging techniques such as Magnetic Resonance Imaging (MRI), Positron Emission Tomography (PET), etc., can visually monitor tumor morphology and metabolic changes, providing an objective basis for evaluating treatment efficacy [7]. [8] found that LD alleviated cisplatin-induced anorexia in rats by inhibiting the PERK/eIF2α/ATF4/CHOP pathway and GDF15/GFRAL expression. This provided a new mechanism explanation for the application of LD in tumor treatment. Sun et al. conducted a systematic review and meta-analysis to investigate the efficacy of LD in treating chronic gastritis, and further revealed its multi-target mechanism of action in digestive system diseases [9].

At present, the research on combining NetP and imaging techniques to explore the intervention of LD in BC is still blank. This study will predict the possible targets and Signaling Pathways (SPs) of LD intervention in BC based on NetP, and dynamically observe its effects on tumor growth and metastasis using imaging techniques. Its aim is to elucidate the material basis and action mechanism of LD in the intervention of BC, provide a scientific basis for the application of TCM in the precision treatment of tumors, and explore a new path of combining TCM and Western medicine to prevent and treat BC.

2 Methods and Materials

2.1 Screening of AIgs and related targets of LD drugs

The chemical composition of LD was qualitatively analyzed utilizing Ultra Performance Liquid Chromatography (UPLC) - Quadrupole Time-of-Flight Tandem Mass Spectrometry. Compounds were identified utilizing databases such as MassBank, PubChem, ChemSpider, TCM Systems Pharmacology (TCMSP), and relevant literature [10]. Meanwhile, a quantitative analysis method was established using UPLC to quantitatively analyze specific components in LD [11]. Through TCMSP, the chemical components of LD were gained, and oral bioavailability (OB $\geq$ 30%) and drug similarity (DL $\geq$ 0.18) were set as filter criteria to identify potential Active Ingredients (AIg) [12]. The related targets of the AIg were queried in the Swiss Target Prediction database, and the species was set as human, followed by outputting the top 100 targets. Meanwhile, through the databases including GeneCards, Online Mendelian Inheritance in Man (OMIM), PharmGkb, TTD, and DrugBank, relevant disease targets were collected. The AIg targets were made a comparison with disease targets, and the common targets between the AIg and the disease were analyzed using online tools such as Venny.

2.2 Retrieval of BC related targets

The keyword "breast cancer" was entered into the GeneCards database to screen for highly correlated genes. Genetic BC related genes were searched in the OMIM database, such as BRCA1/2, PALB2, and PTEN [13]. The "breast neoplasms" were entered into the DisGeNET database to screen for high-confidence gene targets. To obtain the latest research progress, "breast cancer AND therapeutic target" was used as a search strategy in the PubMed database, and literature published in the past 5 years was limited for systematic analysis to supplement potential novel therapeutic targets [14]. The obtained target proteins were stored in Excel for merging and deduplication to obtain the disease target of BC.

2.3 Acquisition of Intersection Target of LD-BC

After obtaining the drug target and disease target through the above steps, they were integrated and Venny 2.1 was taken to draw a Venny diagram to gain the drug disease common target.

2.4 LD - Composition - Target Protein - BC Network Diagram

The AIgs and their targets selected by the above method were imported into the STRING database, and a network diagram was constructed. The screening was conducted based on a comprehensive score of ≥ 0.9 to ensure significant interactions between the selected targets. During the screening process, isolated targets without interactions were excluded to ensure the quality of the constructed protein-protein interaction network. Network indicators include node degree and maximum group centrality, where the mathematical definition of node degree K_i is shown in formula (1).

$$K_i = \sum_{j=1}^{N} A_{ij} \tag{1}$$

In formula (1), A_{ij} is the adjacency matrix element of the protein-protein interaction network. $A_{ij} = 1$ represents the interaction between target points i and j. N is the total number of nodes in the network. Node degree reflects the number of direct connections of the target in the network and is a basic indicator to measure the coreness of the target. The study sets a comprehensive score of ≥0.9 to screen interacting targets and exclude isolated nodes ($K_i = 0$) to mathematically ensure the connectivity and biological significance of the network. The mathematical definition of the maximum group centrality MCC_i is shown in formula (2).

$$MCC_i = \sum_{C \in \varsigma, i \in C} 2^{|C|-1} \tag{2}$$

In formula (2), ς is the set of all cliques (complete subgraphs) in the network. $|C|$ is the number of nodes in the clique. Maximum cluster centrality reflects the degree to which the target participates in the largest complete subgraph and is a key indicator for identifying core Hub genes in the network.

2.5 GO and KEGG Enrichment Analysis

The point information was input into the Metascape database for GO and KEGG enrichment analysis of the targets of LD on BC [15].

2.6 Imaging Examination Methods and Data Analysis

This study included 500 BC patients, all of whom were diagnosed by pathology and received treatment with LD. The age range of patients was 30 to 75 years, with a median age of 52 years. Inclusion criteria: (1) Pathological diagnosis of BC; (2) Patients who have received LD treatment for at least one month; (3) Capable of completing necessary imaging examinations. Exclusion criteria: (1) Presence of concurrent malignant tumors; (2) Other diseases that may affect the results of imaging examinations; (3) Refusal to participate in this study.

All cases underwent MRI examination and were imaged using a 3.0T MRI scanner. Before the examination, the patient needed to fast for 4 hours and remain still during the examination. Before imaging, the scanning parameters were simulated and optimized. According to the estimated preoperative lesion size (≤2 cm, 2-5 cm, >5 cm), the scanning fields of view of 18×18 cm, 20×20 cm, and 22×22 cm were correspondingly set to ensure that the lesion was completely included in the scanning range. Spectral saturated fat suppression technology was simultaneously used for preprocessing to suppress high-signal interference from breast adipose tissue, improve the contrast between lesions and normal glands, and reduce false positive judgments. The examination sequence includes T1/T2-Weighted Imaging (T1WI/T2WI), Diffusion Weighted Imaging (DWI), and Dynamic Contrast Enhanced MRI (DCE-MRI) [16]. T1WI uses a fast spin echo sequence with a Time of Repetition (TR) of 500 ms, a Time of Echo (TE) of 15 ms, a layer thickness of 5 mm, and a layer spacing of 1 mm [17]. T2WI and DWI utilize fast spin echo sequence and single shot echo planar imaging sequence with TR of 4000 ms and 2500 ms, TE of 90 ms and 70 ms, layer thickness of 5 mm and 5 mm, and interlayer spacing of 1 mm and 1mm [18]. DWI also has b=0 and 1000 s/mm2. DCE-MRI uses a 3D fast gradient echo sequence with a TR of 5 ms, 1.5 ms TE, 3 mm layer thickness, and 0.5 mm interlayer spacing [19]. The contrast agent is gadopentetate meglumine, with a dose of 0.1 mmol/kg and an injection rate of 2 ml/s. Scanning should start immediately after injection, with a total of 6 time phases collected, with a 2-minute interval between each phase. The MRI examination is independently reviewed by 2 radiologists with over 10-year-experience to assess the size, morphology, signal characteristics, and enhancement patterns of the tumor. Molecular typing correlation analysis compares the diagnostic efficacy of MRI in different molecular subtypes of hormone receptor positive (HR+)/human epidermal growth factor receptor 2 negative (HER2-), HR+/HER 2 positive (HER2+),

HR negative (HR-)/HER2-, H -/HER2+ based on immunohistochemical results.

Based on the MRI examination result, diagnostic indicators were calculated. The diagnostic consistency between two radiologists was evaluated using the Kappa statistical method [20]. The sensitivity is calculated as the ratio between the True Positive Cases (TPCs) and the Total Number (TNum) of actual diseased cases. The specificity is determined by the ratio of the case numbers of true negative to the actual TNum of unaffected cases; Positive Predictive Value (PPV) is obtained based on the ratio of the TPCs to the TNum of predicted positive cases; Negative Predictive Value (NPV) is the ratio of the true negative cases to the TNum of predicted negative cases; The False Positive Rate (FPR) is calculated by the ratio of the false positive cases to the TNum of actually unaffected cases; The False Negative Rate (FNR) is the ratio of the false negative cases to the TNum of actual cases of illness [21].

Statistical analysis was performed utilizing SPSS 26.0. The measurement data were denoted as mean ± standard deviation (x-±s). A t-test was utilized for inter-group comparison. The percentage was used to represent count data, and the comparison between groups was carried out by the χ^2 test. The $p<0.05$ indicated a statistically significant result.

3 Results

3.1 Screening of AIgs and target proteins for LD drugs

The quantity and intersection size of AIgs in LD herbal medicine are shown in Figure 1 (Appendix).

Figure 1(a) in Appendix shows the number of effective AIgs in various Chinese Herbs Medicine (CHM) in LD. There is a total of 126 AIgs in LD. Among them, Fuling contains 6, Gancao contains 88, Chenpi contains 5, Banxia contains 11, Renshen contains 17, and Baizhu contains 4. Figure 1(b) in Appendix shows the intersection size of the AIgs of various CHMs in LD. The minimum intersection size of Renshen-Gancao is 1, with Gancao reaching up to 85 and Renshen reaching 85.

3.2 BC Related Targets

The distribution of target numbers in the six databases of BC is shown in Figure 2 (Appendix).

In Figure 2 (Appendix), the GeneCards database has the highest number of targets, 3217. There are 784 GEO databases, 309 PharmGkb databases, 142 DrugBank databases, 168 OMIM databases, and 128 TTD databases. After conducting plagiarism checks on various database targets and removing duplicate targets, the TNum of targets related to BC is ultimately determined to be 3563. After integrating and deduplicating all database targets using the unique function in the R language, a total of 3563 non-redundant BC related targets are obtained.

3.3 LD-BC intersection target

The intersection target Venn diagram of LD-BC generated through the Venny 2.1.0 network platform is shown in Figure 3 (Appendix).

In Figure 3 (Appendix), the TNum of related targets for LD is 241, with 61 unique targets. The TNum of targets related to BC is 3563, and the number of targets unique to BC is 3383. The number of common targets for LD and BC is 180. By using the Venn diagram of the intersection targets of LD-BC, the overlap and differences between LD and BC targets can be intuitively understood. These common targets may be key entry points for the potential mechanism of LD on BC, which will help to explore the therapeutic or intervention effects of LD on BC at the molecular level in the future.

3.4 Network Interaction Diagram Analysis

The active AIg information of the LD drug core in the interaction network is listed in Table 1 (Appendix).

In Table 1 (Appendix), Quercetin has a Node Degree Value (NDV) of up to 120, while Kaempferol has an NDV of 84. The NDVs of these two components are significantly higher than those of the other components. Quercetin and Kaempferol are both derived from Gancao, and this medicinal herb contributes three of the top five components in the LD-Component-Target Protein-BC interaction network, including Quercetin, Kaempferol, and Naringenin. This indicates that Gancao is the main material basis source for the anti BC effect of LD. The distribution of NDVs shows a clear grading of the importance of these AIgs in the interaction network as a whole. The components with high NDVs are located at the core, while the components with NDVs around 20 are relatively located at the secondary core or periphery. The detailed information table of some targets is shown in Table 2 (Appendix).

In Table 2 (Appendix), LD treatment for BC involves multiple targets of action. Prostaglandin-related synthase includes PTGS1 and PTGS2. Hormone receptors include ESR1, AR, PPARG, ADRB2, etc. Cell cycle-related proteins include CCNA2 and CDK2. Kinases include CHEK1,

MAPK14, GSK3B, etc. Enzymes include NOS2, PRSS1, DPP4, etc. Ionic channel proteins include SCN5A and KCNH2. The receptor co-activators include NCOA1 and NCOA2. Receptors include RXRA, CHRM1, KDR, and F7.

3.5 GO Function Enrichment Analysis

Biological Process (BP) refers to a continuous biological event driven by molecular function. These events have clear starting and ending nodes, accompanied by dynamic changes in the state of cells or organisms. For the convenience of research and discussion, the selected BP is simply defined. The reaction between estradiol and ethanol is defined as A and B. C, D, E, and F represent the response to hypoxia, aging, lipopolysaccharides, and drugs. G refers to the positive regulation of gene expression. H represents angiogenesis. "I" means the negative regulation of the apoptosis process. J and K are positive regulators of transcriptional DNA templating and cell proliferation. The process of apoptosis is L. The RNA Polymerase II Promoter Transcription Regulation (RNA-pII-PTR) is M, inflammation response is N, and negative regulation of cell proliferation is O. P refers to protein phosphorylation. Q is the positive regulation of the oxidation-reduction process. Signal transduction is defined as R. The negative regulation of RNA-pII-PTR is S. T indicates the Transcription, DNA-templated. The specific bubble diagram of BP is exhibited in Figure 4 (Appendix).

In Figure 4 (Appendix), the BP entries mainly include RNA-pII-PTR, Positive Regulation of Cell Proliferation (PRoCP), and angiogenesis, etc. Cellular Component (CC) refers to the localization of gene products in a cell, that is, where they exist or are associated with which cellular structures. The CC obtained through screening is defined as follows: membrane raft (A1), nuclear chromatin (B1), protein complex (C1), extracellular space (D1), cell surface (E1), cytoplasmic perinuclear region (F1), mitochondria (G1), endoplasmic reticulum membrane (H1), endoplasmic reticulum (I1), cytoplasm (J1), extracellular region (K1), nucleoplasm (L1), Golgi apparatus (M1), plasma membrane components (N1), intracellular (O1), extracellular vesicles (P1), membrane (Q1), plasma membrane (R1), cytoplasm (S1). The CC bubble chart is shown in Figure 5 (Appendix).

In Figure 5 (Appendix), the CC entries mainly include dendrites, nuclei, cytoplasm, and so on. Molecular Function (MF) refers to the specific biochemical activities performed directly by a single gene product at the molecular level, rather than its involvement in BP or localization. The definitions of MF obtained through screening in Figure 5(c) in Appendix: protein binding (A2), enzyme binding (B2), identical protein binding (C2), Sequence Specific-DNA Binding (SS-DNA-B) (I2), ATP binding (E2), DNA binding (F2), protein homodimerization activity (G2), zinc ion binding (H2), transcription factor activity SS-DNA-B (D2), and protein heterodimerization activity (G2). The top 10 Go feature enrichment analysis bar chart is shown in Figure 6 (Appendix).

Figure 6(a) in Appendix shows the enrichment score of BP. The enrichment score for RNA-pII-PTR is the highest, at 50. In the enrichment score of CC in Figure 6(b) (Appendix), the enrichment score of the cell nucleus is the highest, at 84. In the MF enrichment score of Figure 6(c) (Appendix), the protein binding enrichment score is the highest, at 148.

3.6 KEGG Enrichment Analysis

The KEGG pathway enrichment analysis was sorted based on the "-lg P" value, and the top 20 KEGG pathways were analyzed using a bubble plot, as shown in Figure 7 (Appendix).

In Figure 7 (Appendix), the main SPs of KEGG include cancer pathway, MAPK SP, Ras SP, etc. The KEGG pathway analysis bar chart is shown in Figure 8 (Appendix).

In Figure 8 (Appendix), the cancer pathway in human diseases has a high gene enrichment level of 58, which is the highest among all pathways. In environmental information processing, the gene enrichment level of the PI3K Akt SP is the highest, at 34. The gene enrichment degree of focal adhesion in cellular processes is 23.

3.7 Construction of the Intersection Target Core Network and Analysis of Key (Hub) Gene Targets

To deeply analyze the modular structure in the network, this study used the Molecular Complex Detection (MCODE) plugin to perform cluster analysis on the PPI network. Through MCODE analysis, the two functional clusters with the highest scores were identified and selected. The first cluster contains 18 nodes and 55 edges, with an MCODE score of 6.471. This cluster is composed of a series of core targets, including RB1, CDKN1A, AKT1, JUN, CDK2, and Mitogen-activated protein kinase 14 (MAPK14). The second cluster includes 37 nodes and 97 edges, with an MCODE score of 5.389, mainly composed of Hub targets such as STAT3, TP53, RXRA, and MYC. Table 3

(Appendix) provides detailed information on Hub targets.

In Table 3 (Appendix), the NDV of JUN is 15, and the maximum cluster centrality is 20448. The NDV of TP53 is 14, with a maximum cluster centrality of 18744. The nodal degree value of Mitogen-activated protein kinase 3 (MAPK3) is 13, and the maximum cluster centrality is 19,200. Their NDVs and maximum cluster centrality are relatively high, and they may be at the core of the LD treatment network for BC. They interact with many other genes or targets and may be essential in the mechanism of LD in treating BC. Hub genes refer to genes that are vital in BPs. The regulation of other genes is often influenced by this gene. The expression levels of Hub targets in BC tissues are compared, as shown in Figure 9 (Appendix).

Figure 9(a) (Appendix) shows the GEPIA analysis of JUN, TP53, MAPK3, and Cellular Oncogene (FOS). JUN and FOS show low expression in BC. Figure 9(b) (Appendix) shows the GEPIA analysis of MAPK14, MAPK1, MYC, and Ethylene-reactive transcription factor (ESR1). MYC shows low expression in BC, while ESR1 shows high expression in BC. Figure 9(c) in Appendix shows the GEPIA analysis of MAPK8, STAT3, AKT1, and G1/S-specific cyclin D1 (CCND1). CCND1 is highly expressed in BC. In the GEPIA analysis of Figure 9(d) (Appendix), there is $p>0.05$ in the expression levels of RELA, Glucocorticoid receptor (NR3C1), CDKN1A, and RB1 in BC tissue compared to normal tissue. The results of gene correlation analysis are shown in Figure 10 (Appendix).

In the correlation analysis between ESR1 and JUN in Figure 10(a) (Appendix), ESR1 and JUN show a negative correlation. Figure 10(b) (Appendix) displays the correlation analysis between ESR1 and FOS, with a negative correlation between the two. In Figure 10(c) and Figure 10(f) in Appendix, ESR1 and MYC, CCND1 and JUN, CCND1 and FOS, as well as CCND1 and MYC, are negatively correlated with each other. The SPs involved in Hub targets can regulate cell cycle progression, induce apoptosis, and inhibit the invasion and metastasis ability of tumor cells. The survival analysis is shown in Figure 11 (Appendix).

Figure 11(a) (Appendix) shows the survival analysis of JUN and FOS. The survival analysis of BC patients in JUN shows $p>0.05$. The p-value of FOS is 2.1e-05. Figure 11(b) (Appendix) shows the survival analysis of MYC, ESR1, and CCND1, while the survival analysis of BC cases in MYC is $p>0.05$. The p-value of ESR1 is 2.2e-07, which is associated with poor prognosis in BC patients and is highly expressed. The p-value of CCND1 is 0.17.

3.8 Evaluation of the Effectiveness of LD Intervention in BC Patients based on Imaging

The MRI evaluation results of different molecular subtypes after LD intervention are shown in Table 4 (Appendix).

In Table 4 (Appendix), after Liujunzi Decoding intervention in BC patients, the consistency of MRI detection is 83.0%, sensitivity is 95.8%, specificity is 28.4%, FPR is 71.6%, FNR is 4.2%, PPV is 85.1%, and NPV is 61.4%. Further molecular typing analysis shows significant inter-group differences in MRI diagnostic consistency, $p<0.001$. In descending order of consistency, there are: HR+/HER2- > HR+/HER2+ > HR-/HER2- > HR-/HER2+. The HR+/HER2- subtype shows the optimal PPV at 98.0%, but the lowest NPV at 30.8%. The NPV of HR-/HER2- subtype is the highest, at 83.3%. The PPV of HR-/HER2+ subtype is significantly lower than other subtypes, at 70.6%, and there is $p<0.05$ in inter-group. To verify the reliability and accuracy of MRI indicators, 50 BC patients are selected for repeated MRI testing (with an interval of 72 hours, and the testing conditions are completely consistent). The measurement error, Coefficient of Variation (CV), and 95% Confidence Interval (95%CI) of each imaging indicator are calculated. A coefficient of variation $CV < 10\%$ is considered a small measurement error and a stable indicator; $10\% \leq CV \leq 20\%$ is considered an acceptable error; $CV > 20\%$ is considered an unstable indicator. The error analysis results are shown in Table 5 (Appendix).

In Table 5 (Appendix), the CV of all MRI indicators is <10%, among which T2WI signal intensity's CV is the lowest (0.81%), and DCE-MRI enhancement amplitude's CV is the highest (3.51%), but they are all within a stable range. The measurement error of the two repeated measurements is small, and the 95%CI is narrow, indicating that the selected MRI indicators have good measurement repeatability and controllable errors, and can stably reflect the tumor imaging characteristics of BC patients after LD intervention. This result provides a reliable detection basis for subsequent efficacy evaluation.

4 Discussion and Conclusion

4.1 Discussion

The above research results indicate that there are a large number of AIgs in Gancao and Renshen in LD, and the intersection size between the two is relatively large, indicating that they may be crucial in LD. Gancao has various pharmacological effects, such as anti-inflammatory, antioxidant, immune regulation, etc. Renshen is known for its effects, such as replenishing qi, anti-fatigue, and enhancing immunity. The two may enhance the overall efficacy of the formula through synergistic effects in LD. In addition, other herbs such as Banxia, Fuling, Chenpi, and Baizhu have also contributed some AIgs, which may play a role in different pathophysiological processes and together form the pharmacological basis of LD. Y. W. Shang et al. revealed the multi-target regulatory role of LD in the treatment of esophageal cancer through serum metabolomics research. This discovery provided important evidence for this study [22]. LD shares 180 common targets with BC, indicating that LD may intervene in BC through multiple pathways. These common targets may involve multiple key processes like cell invasion, apoptosis, and metastasis. For example, certain targets may be related to cell cycle regulation, and LD inhibits cancer cell proliferation by regulating the activity of these targets. Other targets may be related to the apoptotic pathway, and LD may induce cancer cell apoptosis by activating these targets. W. Huang et al. found in their study on the mechanism of action of similar TCM formulas that LD can affect the biological behavior of tumor cells by regulating relevant targets [23].

BP analysis showed that LD intervenes in BC by regulating RNA-pII-PTR, PRoCP, and angiogenesis. M. Y. Liu et al. pointed out in their study on treating chronic atrophic gastritis with LD in Xiangsha that key BP regulation is of great significance for disease treatment [24]. The RNA-pII-PTR is a key link in gene expression, and its abnormalities are associated with tumor occurrence and development. LD may use this to affect gene expression in BC cells and inhibit tumor proliferation and metastasis. CC analysis shows that LD may act on CC in the nucleus, dendrites, cytoplasm, etc. A. Lahiri et al. found that abnormal regulation of nuclear-related genes is associated with the development of triple-negative BC stem cells. LD can inhibit tumor cell proliferation by affecting gene expression and the cell cycle through its action on the nucleus [25]. MF analysis shows that LD exerts intervention effects through protein binding, transcription factor binding, and other MF pathways. KEGG pathway enrichment analysis shows that it mainly inhibits BC, regulates cell proliferation, apoptosis, and other related genes and SPs by intervening in cancer pathways [26]. NetP research constructs an intersection target core network to screen out JUN, while LD may regulate key hub genes such as TP53. Sun et al. pointed out that LD may act as a key gene for cell cycle and apoptosis by regulating the high NDV of TP53 in the network. LD can inhibit tumor proliferation and induce apoptosis by regulating its expression [27]. GEPIA analysis shows that ESR1 and cyclin D1 are highly expressed in BC. Zhong et al. emphasized that gene expression differences are related to pathological processes, and high expression of ESR1 may be associated with resistance to endocrine therapy, while LD can regulate its expression [28]. Kaplan Meier Plotter survival analysis shows that the expression levels of FOS and ESR1 affect the prognosis of BC, while LD may improve patient prognosis by regulating key gene expression [29].

Quantitative analysis based on MRI imaging evaluation showed that the detection consistency of LD intervention in BC reached 83.0%, with a specificity of only 28.4%, indicating a high risk of FPR judgment. According to S. Beremauro and C. Girio Fragkoulakis' research on BC imaging diagnostic techniques, the phenomenon of insufficient detection specificity is closely related to the inherent high molecular heterogeneity of BC [30]. This is because the individual differences in gene expression, SP activation, and other aspects of tumor cells lead to significant differences in the response of different patients to the same intervention measure, which in turn interferes with the accuracy of imaging detection. The core evaluation basis for the stability of statistical indicators related to MRI diagnosis in the study is repeated measurement error analysis and verification of differences between groups, while sensitivity is reflected by the differences in indicators of different molecular subtypes. In terms of stability, repeated testing results based on 50 patients showed that the CV values of each imaging index were <10%, indicating that the measurement stability of the imaging index itself is excellent, thus ensuring the reliability of statistical index calculations. Compared with current BC imaging, although mammography is convenient and low-cost, it has low sensitivity for dense breasts, contains radiation, and cannot be repeatedly tested in a short period to complete stability verification. Ultrasound imaging has no radiation but low resolution, strong subjectivity, CV value far exceeding 10%, and

insufficient stability. The 3.0T MRI used in the study has both stability and sensitivity, making up for the core shortcomings of alternative methods. At the same time, it is also necessary to objectively acknowledge the shortcomings of too-long detection time and provide a clear direction for subsequent method optimization.

4.2 Conclusion

This study systematically revealed the multidimensional mechanism and clinical effects of LD intervention in BC through a combination of NetP and imaging evaluation. Research has found that LD precisely regulates RNA-pII-PTR, PRoCP, and other BP through multi-component multi-target synergistic effects, targeting CC structures, such as nucleus and cytoplasm. It exerted MF such as protein binding and transcription factor regulation, intervened in key signaling networks such as cancer pathways and PI3K-Akt, and achieved comprehensive regulation of biological behaviors, including BC cell proliferation, apoptosis, invasion, and metastasis. The imaging evaluation results provided clinical evidence supporting the above mechanism. MRI examination showed that the overall consistency of LD intervention was 83.0%, confirming its effectiveness in treating BC. This study not only confirms the clinical application value of LD but also reveals the impact of BC molecular heterogeneity on therapeutic efficacy. In summary, this study systematically elucidates the scientific connotation of LD intervention for BC from the perspectives of molecular mechanisms and clinical efficacy, providing a theoretical basis and practical guidance for the precise application of TCM in the treatment of BC. Future research can further validate the function of key targets through basic experiments, combine multi-omics techniques to deeply analyze the mechanism of action, and conduct large-scale clinical studies to evaluate the effectiveness of their combination therapy, promoting the innovative development of TCM in the field of BC treatment.

Declaration of Generative AI and AI-assisted Technologies in the Writing Process

During the preparation of this work, the author(s) utilized artificial intelligence (AI) technologies solely for the purpose of linguistic refinement and grammatical correction. Following the application of these tools, the author(s) comprehensively reviewed, verified, and edited the resulting text. The author(s) maintain full accountability and responsibility for the accuracy, integrity, and final content of the publication.

References:

[1] T. Meirson, D. A. Goldstein, B. Gyawali, and I. F. Tannock, Review of the monarchE trial suggests no evidence to support use of adjuvant abemaciclib in women with breast cancer, *Lancet Oncol.,* Vol. 24, No. 6, 2023, pp. 589-593. DOI: 10.1016/S1470-2045(23)00165-1.

[2] Z. Hu, F. Wei, Y. Su, Y. Wang, Y. Shen, Y. Fang, et al., Histone deacetylase inhibitors promote breast cancer metastasis by elevating NEDD9 expression, *Signal Transduct. Target,* Vol. 8, No. 2, 2023, pp. 692-704. DOI: 10.1038/s41392-022-01221-6.

[3] Y. Li, L. Y. Ren, H. Xu, J. Liu, H. Y. Li, and F. L. Zhu, Effect of Xiangsha Liujunzi decoction combined with entecavir on T cell subsets in patients with decompensation period of hepatitis B cirrhosis, *Chin. J. Integr. Tradit. West. Med. Dig.,* Vol. 32, No. 1, 2024, pp. 35-41. DOI: 10.3969/j.issn.1671-038X.2024.01.07.

[4] L. Zhang, D. Ma, and W. D. Shan, Effect of Sijunzi decoction on the myonuclear domain of rat soleus in spleen qi deficiency, *Chinese Med.,* Vol. 14, No. 4, 2023, pp. 276-285. DOI: 10.4236/cm.2023.144015.

[5] N. Z. Ismail, M. Khairuddean, S. Abubakar, and H. Arsad, Network pharmacology, molecular docking and molecular dynamics simulation of chalcone scaffold-based compounds targeting breast cancer receptors, *J. Biomol. Struct. Dyn.,* Vol. 43, No. 7, 2023, pp. 3242-3257. DOI: 10.1080/07391102.2023.2296606.

[6] P. Mirosawa, A. Konieczna, K. Widerska, et al. Treatment outcomes and prognostic factors in nonmetastatic metaplastic breast cancer patients: A multicenter retrospective cohort study, *Acta Oncol.,* Vol. 63, No. 1, 2024, pp. 620-635. DOI: 10.2340/1651-226X.2024.40413.

[7] M. Kataoka, M. Iima, K. K. Miyake, and M. Honda, Multiparametric approach to breast cancer with emphasis on magnetic resonance imaging in the era of personalized breast cancer treatment, *Invest. Radiol.,* Vol. 59, No. 1, 2024, pp. 26-37. DOI: 10.1097/RLI.0000000000001044.

[8] Y. Dai, W. Hu, J. Han, Y. Zhao, X. Wu, X. Liao, et al. Liujunzi decoction attenuates cisplatin-induced anorexia in rats via inhibiting PERK/eIF2α/ATF4/CHOP pathway and GDF15/GFRAL expression, *J. Holist. Integr. Pharm.,* Vol. 5, No. 2, 2024, pp. 113-120, May, 2024, DOI: 10.1016/j.jhip.2024.05.002.

[9] Z. Sun, H. Deng, and J. Liu, A systematic review and meta-analysis of Xiangsha Liujunzi decoction in the treatment of chronic gastritis, *Comb. Chem. High Throughput Screen.,* Vol. 27, No. 3, 2024, pp. 386-399. DOI: 10.2174/0113862073252121230925103843.

[10] W. Shu, Z. Wang, R. Zhao, R. Shi, J. Zhang, W. Zhang, and H. Wang, Exploration of the effect and potential mechanism of Echinacoside against endometrial cancer based on network pharmacology and in vitro experimental verification, *Drug Des. Dev. Ther.,* Vol. 16, 2022, pp. 1847-1863. DOI: 10.2147/DDDT.S361955.

[11] S. Shreya, D. N. Kumar, D. Mohapatra, S. Jaiswal, G. G. Naik, S. K. Guru, and A. N. Sahu. Tracing the anti-cancer mechanism of Pleurotus Osteratus by the integrative approach of network pharmacology and experimental studies, *Appl. Biochem. Biotechnol.,* Vol. 195, No. 1, 2023, pp. 152-171. DOI: 10.1007/s12010-022-04111-3.

[12] J. Gao, S. Yang, G. Xie, J. Pan, and F. Zhu, Integrating network pharmacology and experimental verification to explore the pharmacological mechanisms of aloin against gastric cancer, *Drug Des. Dev. Ther.,* Vol. 16, 2022, pp. 1947-1961. DOI: 10.2147/DDDT.S360790.

[13] A. M. Elasbali, W. A. Al-Soud, A. E. Mousa Elayyan, Z. H. Al-Oanzi, H. H. Alhassan, B. M. Mohamed, and M. Adnan, Integrating network pharmacology approaches for the investigation of multi-target pharmacological mechanism of 6-Shogaol against cervical cancer, *J. Biomol. Struct. Dyn.,* Vol. 41, No. 23, 2023, pp. 14135-14151. DOI: 10.1080/07391102.2023.2191719.

[14] M. H. H. Mohammed, A. N. E. Hamed, S. F. Elhabal, F. A. Mokhtar, U. R. Abdelmohsen, and M. A. Fouad, Metabolic profiling and cytotoxic activities of ethanol extract of Dypsis Leptocheilos aerial parts and its green synthesized silver nanoparticles supported by network pharmacology analysis, *S. Afr. J. Bot.,* Vol. 161, 2023, pp. 648-665. DOI: 10.1016/j.sajb.2023.06.007.

[15] D. Luo, H. Liu, X. Liang, W. Yan, C. Ding, C. B. Hu, and J. B. Wu, Analysis of the potential angiogenic mechanisms of Bushenhuoxue decoction against osteonecrosis of the femoral head based on network pharmacology and experimental validation, *Orthop. Surg.,* Vol. 16, No. 3, 2024, pp. 700-717. DOI: 10.1111/os.13970.

[16] B. H. Yan, Q. X. Xu, X. Ge, M. T. Gao, Y. Li, L. Guo, and Y. Pan, Molecular mechanisms of chengshi beixie fenqing decoction based on network pharmacology: Pivotal roles of relaxin signaling pathway and its associated target proteins against benign prostatic hyperplasia, *J. Biomol. Struct. Dyn.,* Vol. 42, No. 4, 2023, pp. 2075-2093. DOI: 10.1080/07391102.2023.2203237.

[17] K. Simon, M. Vicent, K. Addah, D. Bamutura, B. Atwiine, D. Nanjebe, and A. O. Mukama, "Comparison of deep learning techniques in detection of sickle cell disease, AIA, Vol. 1, No. 4, 2023, pp. 252-259. DOI: 10.1080/07391102.2023.2191719.

[18] B. A. Bhat, W. Rashid Mir, M. Alkhanani, A. Almilaibary, and M. A. Mir, Network pharmacology and experimental validation for deciphering the action mechanism of fritillaria cirrhosa d. don constituents in suppressing breast carcinoma, *J. Biomol. Struct. Dyn.,* Vol. 42, No. 23, 2023, pp. 13002-13022. DOI: 10.1080/07391102.2023.2274966.

[19] D. Mankoff, S. Balogova, L. Dunnwald, F. Dehdashti, E. DeVries, L. Evangelista, M. Van Kruchten, S. Carrilho Vaz, A. Fowler, H. Linden, and G. A. Ulaner, Summary: SNMMI procedure standard/EANM practice guideline for estrogen receptor imaging of patients with breast cancer using 16a-[~18F]Fluoro-17b-Estradiol PET, *J. Nucl. Med.,* Vol. 65, No. 2, 2024, pp. 221-223. DOI: 10.2967/jnumed.124.267461.

[20] M. Alvarez-Benito, Imaging evaluation of neoadjuvant breast cancer treatment: Where do we stand? *Eur. Radiol.,* Vol. 34, No. 10, 2024, pp. 6271-6272. DOI: 10.1007/s00330-024-10799-0.

[21] T. Azuma, Current status and outlook of ring type ultrasound imaging system for breast cancer screening, *J. Jpn. Soc. Precis. Eng.,* Vol. 89, No. 1, 2023, pp. 31-35. DOI: 10.2493/jjspe.89.31.

[22] Y. W. Shang, X. Chen, Y. S. Wu, Z. X. Zhou, Y. Liu, Y. R. Liu, and Y. L. Chen, Liujunzi Decoction treats 4NQO-induced esophageal cancer in mice: A study based on serum metabolomics, *Chinese Journal of Traditional Chinese Medicine,* Vol. 49, No. 2, 2024, pp. 461-470. DOI: 10.19540/j.cnki.cjcmm.20231013.702.

[23] W. Huang, F. Wen, S. Ruan, P. Gu, S. Gu, S. Song, and P. Shu, Integrating HPLC-Q-TOF-MS/MS, network pharmacology and experimental validation to decipher the

chemical substances and mechanism of modified Gui-shao-liu-jun-zi decoction against gastric cancer, *J. Tradit. Complement. Med.,* Vol. 13, No. 3, 2023, pp. 245-262. DOI: 10.1016/j.jtcme.2023.05.005.

[24] M. Y. Liu, Y. L. Liang, Y. X. Cheng, Y. Q. Duan, M. Bai, X. M. Yuan, Z. Y. Liu, and Y. X. Gong, Molecular mechanism of Xiangsha Liujunzi Decoction in treating chronic atrophic gastritis based on transcriptome sequencing technology, *Chinese Journal of Traditional Chinese Medicine,* Vol. 49, No. 18, 2024, pp. 4977-4985, DOI: 10.19540/j.cnki.cjcmm.20240509.401.

[25] A. Lahiri, H. Vundavilli, M. Mondal, P. Bhattacharjee, B. Decker, G. Del Priore, and A. Datta, Drug Target identification in triple negative breast cancer stem cell pathways: A computational study of gene regulatory pathways using Boolean networks, *IEEE Access,* Vol. 11, 2023, pp. 56672-56690. DOI: 10.1109/ACCESS.2023.3283291.

[26] H. P. Manivannan, V. P. Veeraraghavan, and A. P. Francis, Identification of molecular targets of Trigonelline for treating breast cancer through network pharmacology and bioinformatics-based prediction, *Mol. Divers.,* Vol. 28, No. 1, 2024, pp. 3835-3857, DOI: 10.1007/s11030-023-10780-x.

[27] M. Sun, F. Lv, C. Qin, W. Li, and S. Liu, The potential mechanism of Liujunzi decoction in the treatment of breast cancer based on network pharmacology and molecular docking technology, *Curr. Pharm. Des.,* Vol. 30, No. 9, 2024, pp. 702-726. DOI: 10.2174/0113816128289900240219104854.

[28] Y. Zhong, B. Wang, W. Chen, H. Zhang, J. Sun, and J. Dong, Exploring the mechanisms of modified Bu-Shen-Yi-Qi decoction for COPD-related osteoporosis therapy via transcriptomics and network pharmacology approach, *Drug Des. Dev. Ther.,* Vol. 17, 2023, pp. 2727-2745. DOI: 10.2147/DDDT.S413532.

[29] H. Xin, M. Wang, S. Wang, H. Han, and N. Jiang, Exploration of potential therapeutic targets of Shentong Zhuyu decoction for ankylosing spondylitis based on network pharmacology and molecular docking, *J. Inflamm. Res.,* Vol. 17, 2024, pp. 6453-6468, DOI: 10.2147/JIR.S453638.

[30] S. Beremauro and C. Girio-Fragkoulakis, Imaging techniques in breast cancer," Surgery (Oxford), Vol. 42, No. 12, 2024, pp. 875-883, DOI: 10.1016/j.mpsur.2024.09.006.

Contribution of Individual Authors to the Creation of a Scientific Article (Ghostwriting Policy)

The authors equally contributed in the present research, at all stages from the formulation of the problem to the final findings and solution.

Sources of Funding for Research Presented in a Scientific Article or Scientific Article Itself

No funding was received for conducting this study.

Conflict of Interest

The authors have no conflicts of interest to declare that are relevant to the content of this article.

Creative Commons Attribution License 4.0 (Attribution 4.0 International, CC BY 4.0)

This article is published under the terms of the Creative Commons Attribution License 4.0
https://creativecommons.org/licenses/by/4.0/deed.en_US

APPENDIX

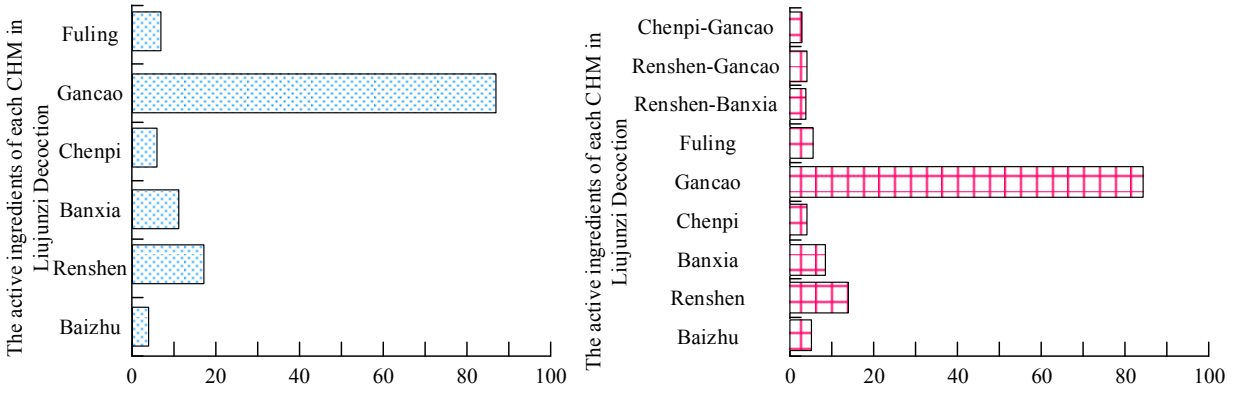


Fig. 1: The quantity and intersection size of AIgs in LD
Source: created by the authors

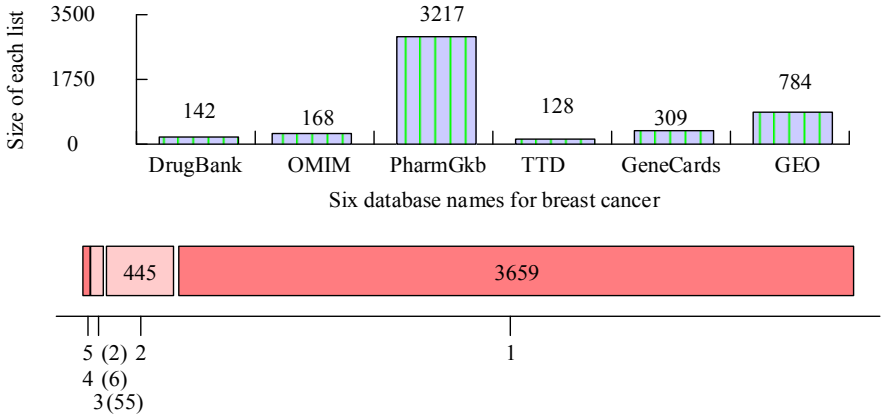


Fig. 2: Target distribution map of six databases in BC
Source: created by the authors

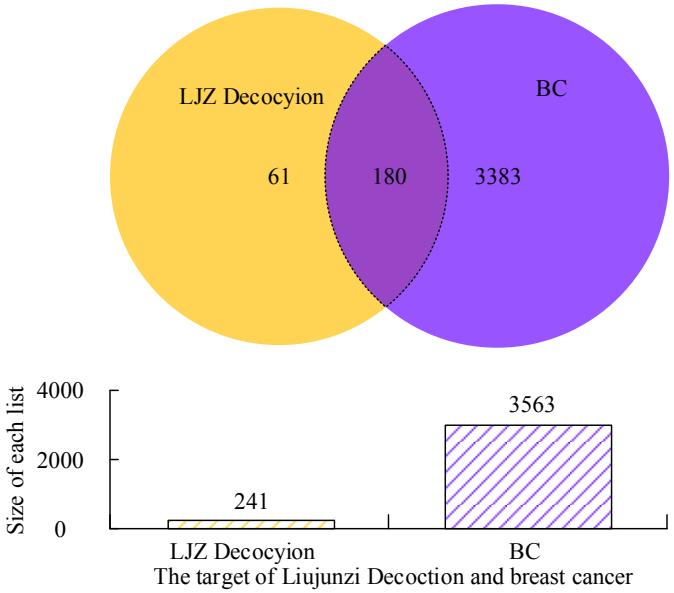


Fig. 3: Venn plot of LD-BC intersection targets
Source: created by the authors

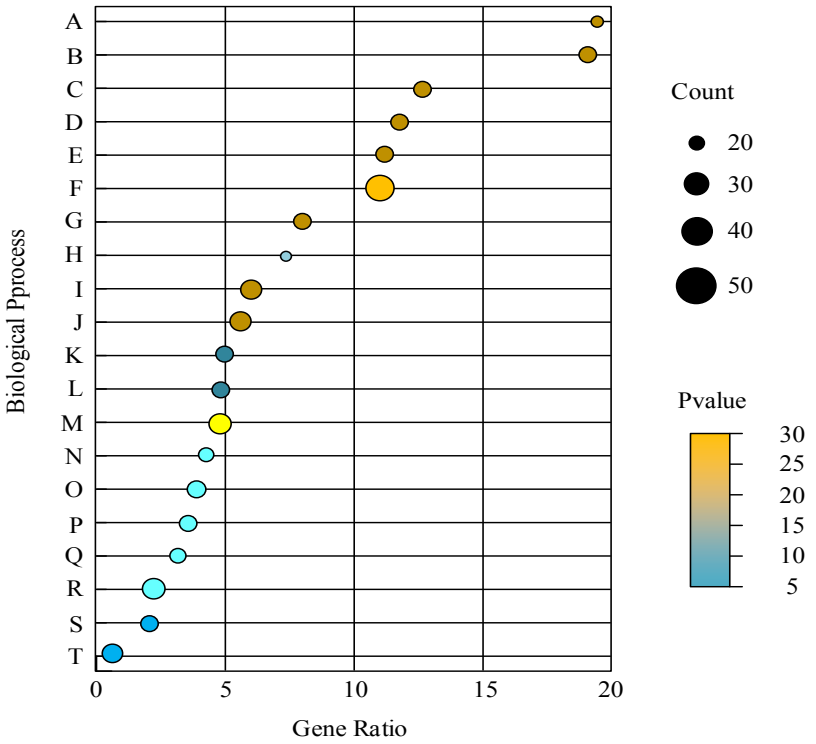


Fig. 4: BP bubble diagram of LD's effect on BC targets
Source: created by the authors

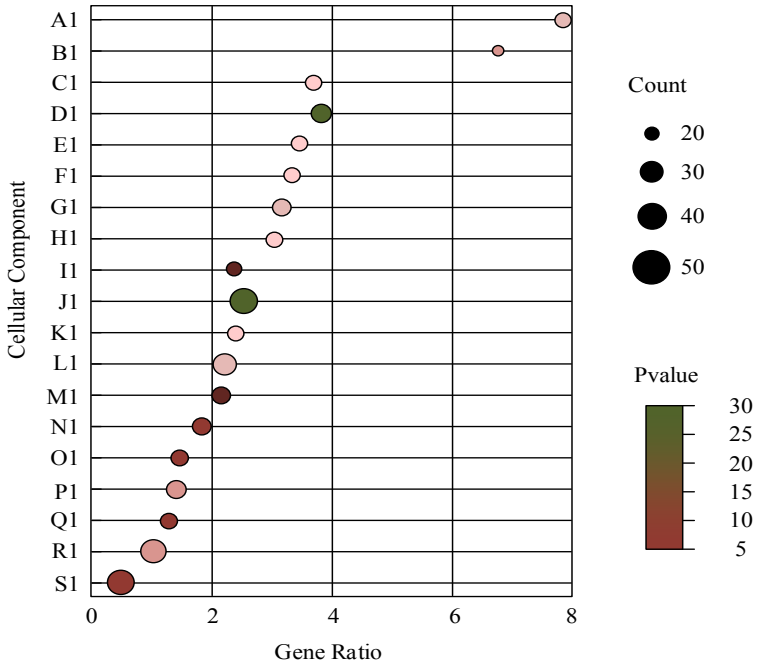


Fig. 5: CC bubble chart of LD's effect on BC targets
Source: created by the authors

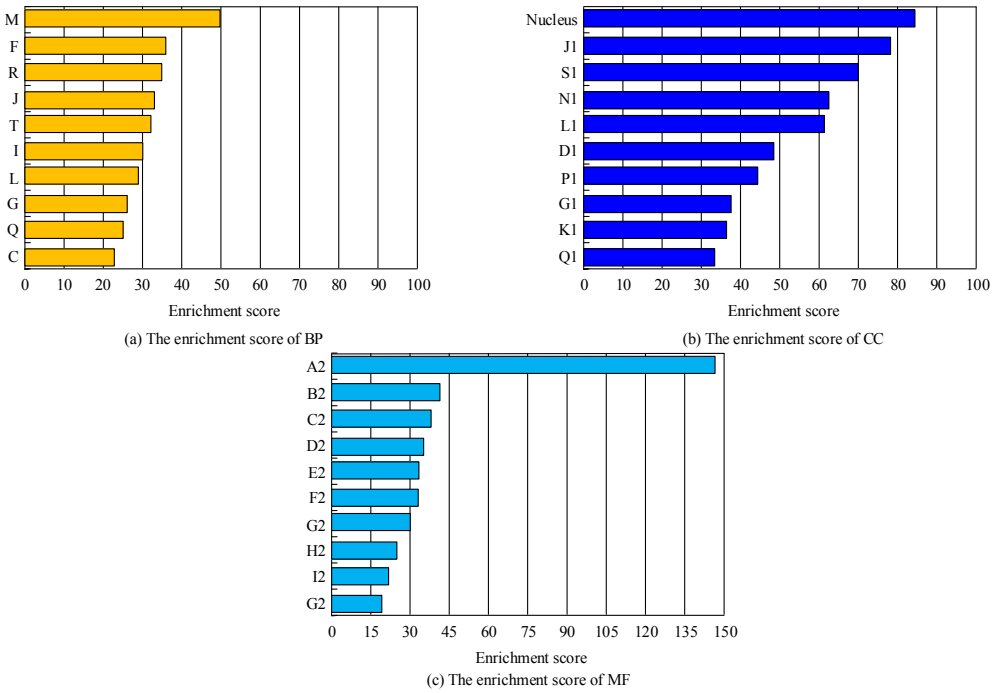


Fig. 6: Bar chart of Go functional enrichment analysis
Source: created by the authors

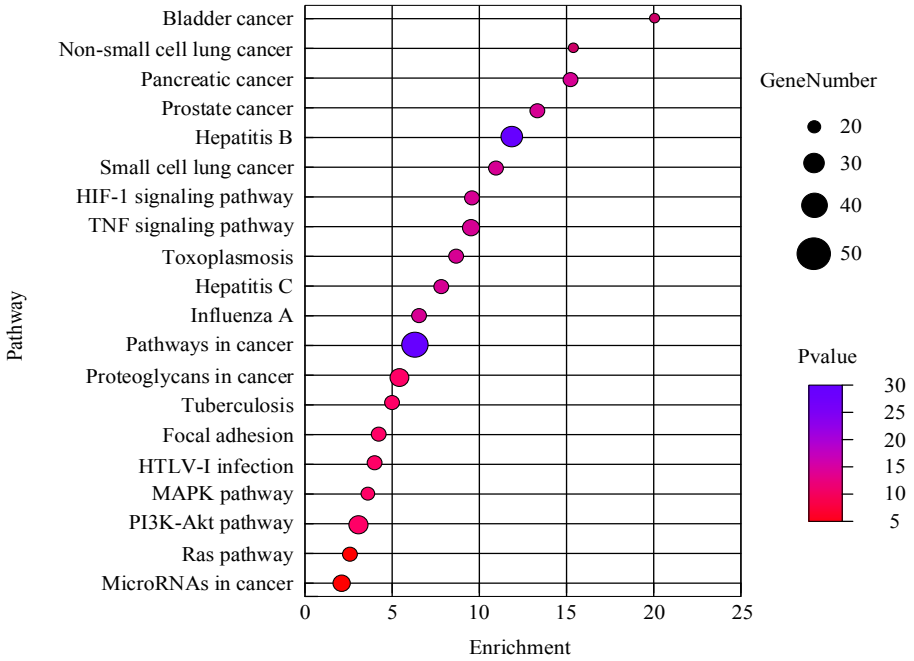


Fig.7: Bubble chart of top 20 ranked KEGG pathway analysis

Source: created by the authors

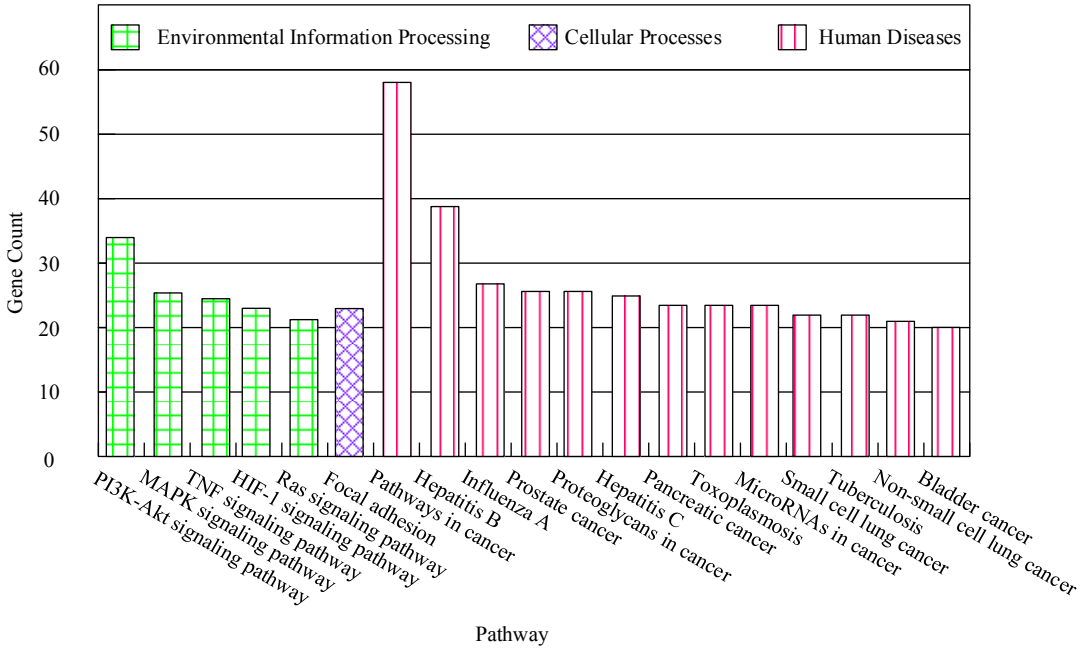


Fig.8: KEGG pathway analysis bar chart

Source: created by the authors

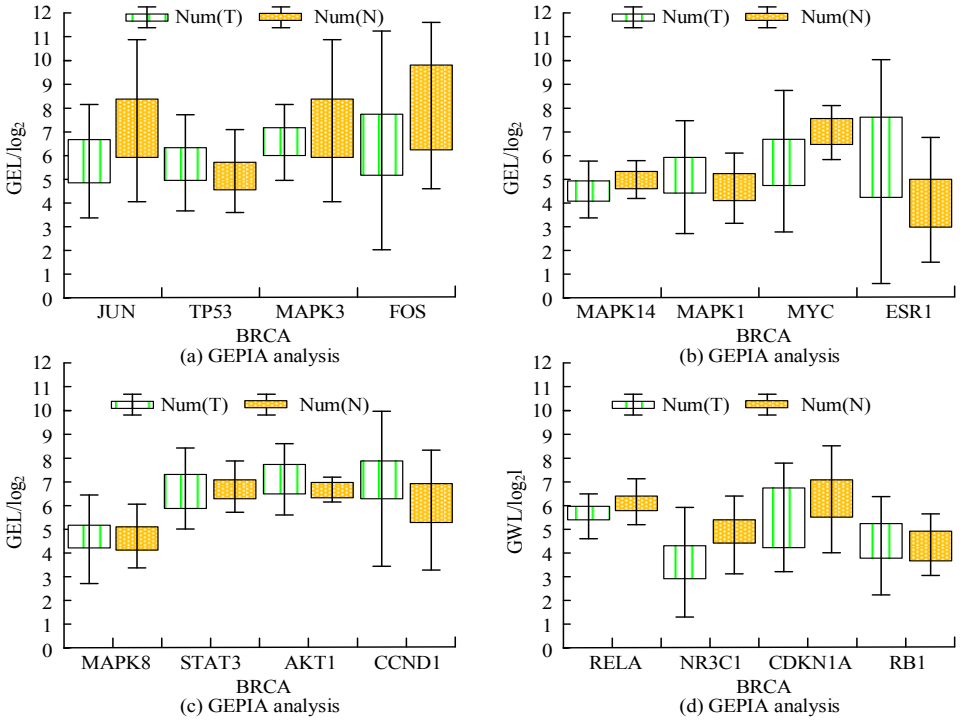


Fig. 9: Comparison of expression levels of Hub targets in BC tissues
Source: created by the authors

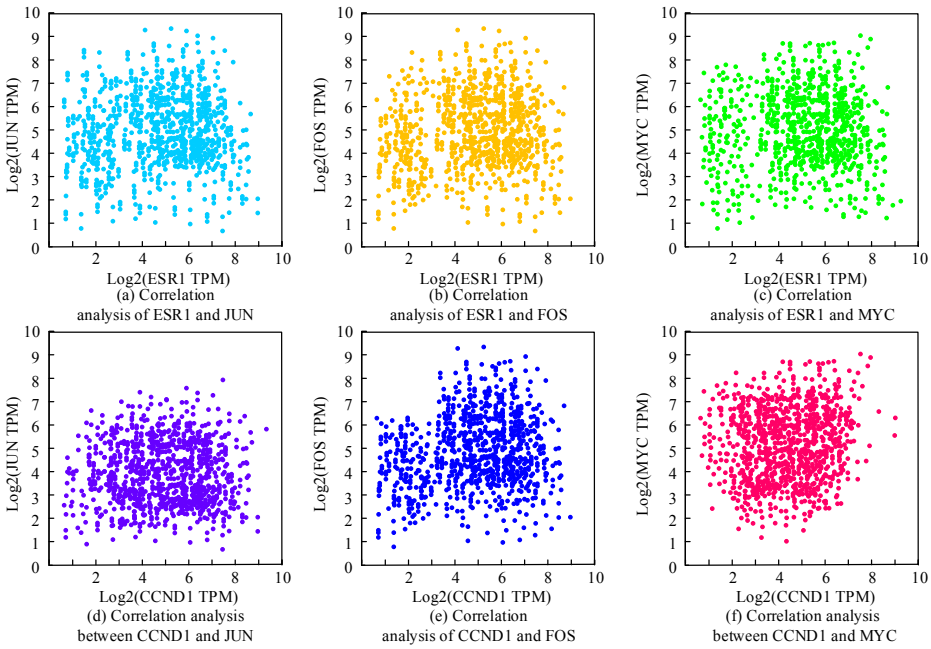
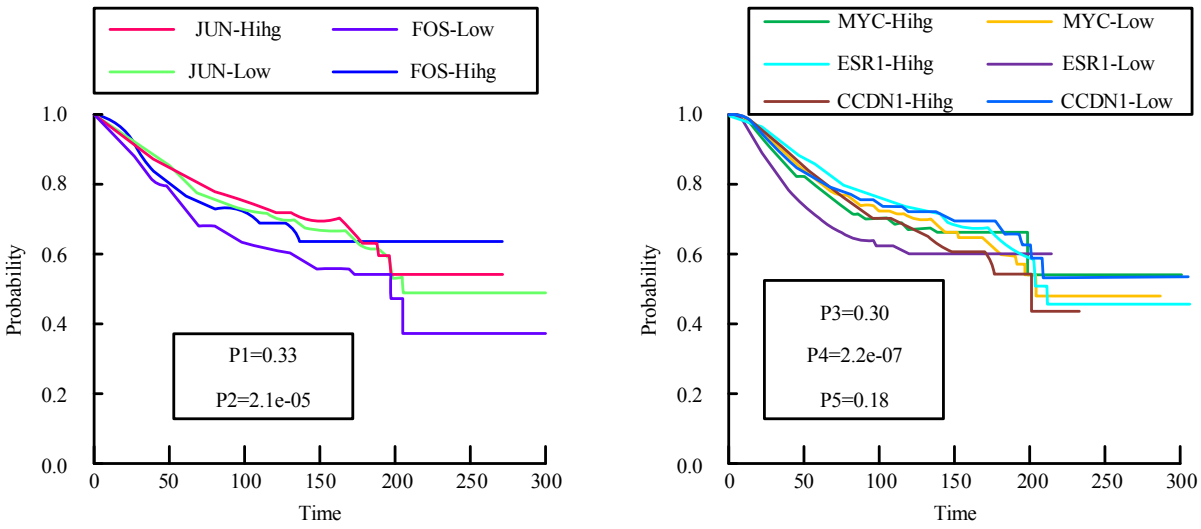


Fig. 10: Correlation analysis diagram of genes
Source: created by the authors



(a) Survival analysis of JUN and FOS (b) Survival analysis of MYC, ESR1 and CCDN1

Fig. 11: Survival analysis of differentially expressed Hub genes in LD in treating BC

Source: created by the authors

Table 1. Details on the AIgs and effective ingredients of the core drug of LD

Compound	NDV	Compound	NDV
Quercetin	120	Shinpterocarpin	22
Kaempferol	84	3'-Hydroxy-4'-O-Methylglabridin	22
Naringenin	53	3'-Methoxyglabridin	22
Beta-sitosterol	41	Glypallichalcone	22
Stigmasterol	34	Vestitol	21
Nobiletin	29	1-Methoxyphaseollidin	21
Baicalein	28	HMO	21
Licochalcone a	27	Licagrocarpin	21
7-Methoxy-2-methyl isoflavanone	26	Medicarpin	20
Formononetin	25	Glabridin	20
DDHPCM	23	Glyasperins M	20
Isohamnetin	22	/	/

Source: created by the authors

Table 2. Some targets in the interaction network

Gene name	Gene abbreviation	NDV	Gene name	Gene abbreviation	NDV
Prostaglandin G/H synthase 2	PTGS2	108	Estrogen receptor β	GSK3B	56
Ethylene-reactive transcription factor	ESR1	81	Cyclin A2	CCNA2	55

Heat shock protein HSP90-beta	HSP90AB1	77	Serine/threonine protein kinase Chk1	CHEK1	48
Androgen receptor	AR	75	Mitogen-activated protein kinase 14	MAPK14	48
Peroxisome proliferators activate receptors	PPARG	68	Beta-2 adrenergic receptor	ADRB2	44
Nitric oxide synthase	NOS2	68	Dipeptidyl peptidase 4	DPP4	41
Nuclear receptor co-activator 2	NCOA2	63	Retinoic acid receptor RXR-alpha	RXRA	37
Sodium channel protein type 5 subprotein	SCN5A	61	Coagulation factor VII	F7	27
Prostaglandin G/H synthase 1	PTGS1	61	Muscarinic acetylcholine receptor M	CHRM1	26
Trypsin 1	PRSS1	59	Nuclear receptor coactivator 1	NCOA1	25
Cyclin-dependent kinase 2	CDK2	58	Potassium voltage gated channel shunt	KCNH2	23
Glycogen synthase kinase 3 beta	GSK3B	58	Receptor protein tyrosine kinase	KDR	20

Source: created by the authors

Table 3. Detailed information about the Hub target

Gene name	Gene abbreviation	NDV	Maximum group centrality
Proto-oncogene activating protein	JUN	15	20448
Cellular tumor antigen p53	TP53	14	18744
Mitogen-activated protein kinase 3	MAPK3	13	19200
Cellular oncogene	FOS	12	16344
Mitogen-activated protein kinase 14/1	MAPK14/MAPK1	12/12	9600/9600
Proto-oncogene protein	MYC	12	7104
Ethylene-reactive transcription factor	ESR1	11	13200
Mitogen-activated protein kinase 8	MAPK8	11	12984
Signal transducer and transcriptional activator 3	STAT3	11	5184
Serine/threonine protein kinase 1	AKT1	11	4080
G1/ S-specific cyclin D1	CCND1	10	1224
RELA proto-oncogene	RELA	9	1704
Glucocorticoid receptor	NR3C1	9	11520
Cyclin-dependent kinase inhibitor 1	CDKN1A	8	864
Retinoblastoma-related proteins	RB1	8	864

Source: created by the authors

Table 4. MRI evaluation of different molecular subtypes after the intervention of LD

Indicator	HR+/HER2- (%)(n=210)	HR+/HER2+ (%)(n=87)	HR-/HER2+(%)(n=105)	HR-/HER2- (%)(n=98)	Total (%)(n=500)	*p* value
Consistency	197/210 (93.8)	68/87 (78.2)	74/105 (70.5)	76/98 (77.6)	415/500 (83.0)	<0.001
Sensitivity	193/202 (95.5)	64/65(98.5)	60/66(90.9)	71/72(98.6)	388/405 (95.8)	0.054
Specificity	4/8(50.0)	4/22(18.2)	14/39(35.9)	5/26(19.2)	27/95(28.4)	0.160
FPR	4/8(50.0)	18/22(81.8)	25/39(64.1)	21/26(80.8)	68/95(71.6)	0.829
FNR	9/202(4.5)	1/65(1.5)	6/66(9.1)	1/72(1.4)	17/405(4.2)	0.054
PPV	193/197 (98.0)	64/82(78.0)	60/85 (70.6)	71/92(77.2)	388/456 (85.1)	<0.001
NPV	4/13(30.8)	4/5(80.0)	14/20(70.0)	5/6(83.3)	27/44(61.4)	0.012

Source: created by the authors

Table 5. Error analysis of MRI indicators (n=50)

Imaging Index	First measurement (Mean±SD)	Second measurement (Mean±SD)	Measurement error (Mean±SD)	CV (%)	95%CI	Stability evaluation
T1WI signal intensity	285.6±32.4	288.9±31.7	3.3±1.8	1.15	(279.2, 295.3)	Stable
T2WI signal intensity	356.8±41.2	359.7±40.8	2.9±2.1	0.81	(351.5, 365.9)	Stable
DWI ADC value ($\times10^{-3}$ mm^2/s)	1.28±0.15	1.31±0.14	0.03±0.02	2.34	(1.25, 1.34)	Stable
DCE-MRI enhancement amplitude (%)	68.5±8.7	70.2±8.5	1.7±1.3	2.48	(67.8, 70.9)	Stable
Tumor size (mm)	25.3±5.6	25.8±5.4	0.5±0.3	1.98	(24.7, 26.4)	Stable
Enhancement time (s)	45.6±6.8	47.2±6.5	1.6±1.2	3.51	(44.9, 47.9)	Stable

Source: created by the author